

Mixed-Valence Cu^I–Cu^{II} and Heterodimetallic Cu^I–M^{II} Bis(carboxylate-bridged) Complexes: Structural, Electrochemical, and Spectroscopic Investigations

Daniel D. LeCloux,[†] Roman Davydov,[‡] and Stephen J. Lippard^{*,†}

Department of Chemistry, Massachusetts Institute of Technology, Cambridge, Massachusetts 02139, and the Department of Chemistry, Northwestern University, Evanston, Illinois 60208

Received July 2, 1998

The synthesis, spectroscopic, electrochemical, and structural properties of a series of Cu^ICu^{II} bis(carboxylate-bridged) complexes are described, together with related investigations of Cu^IM^{II} (M = Fe, Zn) analogues. Treatment of previously reported [Cu₂(XDK)(MeCN)] (**1**) or [Cu₂(PXDK)(MeCN)] (**2**), where H₂XDK = *m*-xylylenediamine bis(Kemp's triacid imide) and H₂PXDK = the propyl derivative of H₂XDK, with 1 equiv of silver(I) triflate, trifluoroacetate, or tetrafluoroborate in THF afforded mixed-valence complexes [Cu₂L(μ-X)(THF)₂], where X = triflate and L = XDK (**4**), PXDK (**5**); X = trifluoroacetate and L = XDK (**6**) and [Cu₂L(THF)₄]X, where X = tetrafluoroborate, L = XDK (**7**), PXDK (**8**). Compound **8** was also prepared from an equimolar mixture of (Et₄N)[Cu(PXDK)] (**3**) and copper(II) triflate. Solid-state structural investigations of **4**, **6**, and **8** revealed symmetric, square pyramidal coordination environments about each copper atom and short Cu–Cu distances ranging from 2.3988(8) to 2.4246(12) Å. These features imply significant metal–metal bonding character, the nature of which was further interrogated. Comparative structural and ligand exchange studies with mixed-metal analogues [CuZn(PXDK)(OTf)(THF)₂(H₂O)] (**9**), [CuFe(PXDK)(OTf)(NB)(MeCN)]₂ (**10**, NB = norbornene), and [CuZn(PXDK)(OTf)(NB)(H₂O)] (**11**) revealed longer metal–metal distances ranging from 3.294(2) to 3.732(2) Å and monodentate, terminal triflate ligation. Variable-temperature and variable-field EPR studies showed that complexes **4–8** have fully delocalized electronic structures in the solid state and solution down to liquid helium temperatures. Molecular orbital calculations on simplified models of **4–8** revealed a Cu–Cu bonding interaction in the SHOMO and SOMO, comprising mainly σ-type overlap between the d_{x²–y²} orbitals. In addition, cyclic voltammetric studies of compound **4** revealed a chemically reversible, electrochemically quasireversible one-electron reduction at a positive potential for a Cu^ICu^{II} complex having a dianionic, oxygen-rich donor set. The relevance of these properties to the electronically similar Cu–Cu bonded system of the biological Cu_A center is discussed.

Introduction

The cellular respiratory protein cytochrome *c* oxidase (CcO) couples the catalytic reduction of dioxygen to water with the production of a proton gradient across the cell membrane, providing the energy essential for ATP synthesis from ADP and inorganic phosphate.¹ Another respiratory protein, nitrous oxide reductase (N₂OR), plays an analogous role in denitrifying bacteria by catalyzing the reduction of N₂O to N₂ and water.² A common feature of these enzymes is their use of a unique electron-transfer center, Cu_A. Recent spectroscopic^{3–8} and X-ray structural^{9–11} studies have provided compelling evidence that

Cu_A is a fully delocalized mixed-valence “class III”¹² dicopper center. Each copper ion is ligated by two bridging cysteine thiolates and a terminal histidine nitrogen atom, with weaker contacts occurring between a methionine thioether and one copper and between a glutamate carboxylate oxygen atom and the other (Table 1). The inter-metal distance of 2.5 Å in Cu_A is consistent with the presence of a metal–metal bond, a feature unprecedented in biological systems and responsible for the highly unusual electronic properties and function of the center.^{13,14}

The recent characterization of the Cu_A site invites comparison with well-defined complexes that model its structural and spectroscopic properties. Many mixed-valence dicopper complexes are known, but most are fully localized class I systems,

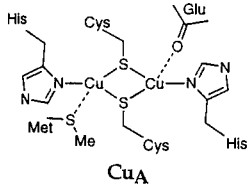
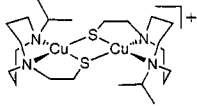
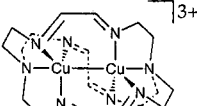
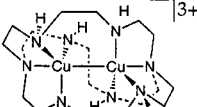
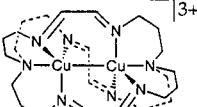
[†] Massachusetts Institute of Technology.

[‡] Northwestern University.

- (1) Ferguson-Miller, S.; Babcock, G. T. *Chem. Rev.* **1996**, *96*, 2889–2907.
- (2) Zumft, W. G.; Kroneck, P. M. H. *FEMS Symp. Ser.* **1990**, *56*, 37–55.
- (3) Blackburn, N. J.; deVries, S.; Barr, M. E.; Houser, R. P.; Tolman, W. B.; Sanders, D.; Fee, J. A. *J. Am. Chem. Soc.* **1997**, *119*, 6135–6143.
- (4) Farrar, J. A.; Neese, F.; Lappalainen, P.; Kroneck, P. M. H.; Saraste, M.; Zumft, W. G.; Thomson, A. J. *J. Am. Chem. Soc.* **1996**, *118*, 11501–11514.
- (5) von Wachenfeldt, C.; deVries, S.; van der Oost, J. *FEBS Lett.* **1994**, *340*, 109–113.
- (6) Neese, F.; Zumft, W. G.; Antholine, W. E.; Kroneck, P. M. H. *J. Am. Chem. Soc.* **1996**, *118*, 8692–8699.
- (7) Lappalainen, P.; Aasa, R.; Malmström, B. G.; Saraste, M. *J. Biol. Chem.* **1993**, *268*, 26416–26421.
- (8) Farrar, J. A.; Thomson, A. J.; Cheesman, M. R.; Dooley, D. M.; Zumft, W. G. *FEBS Lett.* **1991**, *294*, 11–15.

- (9) Iwata, S.; Ostermeier, C.; Ludwig, B.; Michel, H. *Nature* **1995**, *376*, 660–669.
- (10) Tsukihara, T.; Aoyama, H.; Yamashita, E.; Tomizaki, T.; Yamaguchi, H.; Shinzawa-Itoh, K.; Nakashima, R.; Yaono, R.; Yoshikawa, S. *Science* **1995**, *269*, 1069–1074.
- (11) Tsukihara, T.; Aoyama, H.; Yamashita, E.; Tomizaki, T.; Yamaguchi, H.; Shinzawa-Itoh, K.; Nakashima, R.; Yaono, R.; Yoshikawa, S. *Science* **1996**, *272*, 1136–1144.
- (12) Robin, M. B.; Day, P. *Adv. Inorg. Chem. Radiochem.* **1967**, *10*, 247–422.
- (13) Gamelin, D. R.; Randall, D. W.; Hay, M. T.; Houser, R. P.; Mulder, T. C.; Canters, G. W.; deVries, S.; Tolman, W. B.; Lu, Y.; Solomon, E. I. *J. Am. Chem. Soc.* **1998**, *120*, 5246–5263.
- (14) Ramirez, B. E.; Malmström, B. G.; Winkler, J. R.; Gray, H. B. *Proc. Natl. Acad. Sci. U.S.A.* **1995**, *92*, 11949–11951.

Table 1. Summary of Pertinent Spectroscopic and Structural Data on Known Class III Mixed-Valence Copper Systems

Complex	Visible-NIR (λ_{\max} , nm (ϵ , M ⁻¹ cm ⁻¹))	Cu–Cu _i Dist. (Å)	EPR ^b	ref
 CuA	363 (1200), ^a 480 (3000), 532 (3000), 808 (1600)	2.5–2.7	$g_{\min} = 2.003$, ^c $g_{\text{mid}} = 2.005$, $g_{\max} = 2.203$, $A_X^{65\text{-Cu}} = 105$ G, $A_Y^{65\text{-Cu}} = 116$ G, $A_Z^{65\text{-Cu}} = 235$ G	6,7, 9–11
 (CuLiPrdacoS)₂(OTf)	358 (2700), 602 (800), 786 (sh), 1466 (1200)	2.9306(9)	$g_1 = 2.010$, $g_2 = 2.046$, $g_3 = 2.204$, $A_2^{\text{Cu}} = 36.3$ G, $A_3^{\text{Cu}} = 49.9$ G	21
 (Cu₂L¹)³⁺	600–650 (1500–3500), ^d 756 (5000)	2.448 ^e	$g_{\parallel} = 2.004$, $g_{\perp} = 2.148$, $A_{\parallel} = 11$ G, $A_{\perp} = 111$ G	23–24
 (Cu₂L²)³⁺	622 (2900), 736 (4500)	2.415(1)	$g_{\parallel} = 2.02$, $g_{\perp} = 2.15$, $A_{\parallel} = 22$ G, $A_{\perp} = 115$ G	25
 (Cu₂L³)³⁺	600–650 (1500–3500), ^d 750–780 (5000)	2.419(1)	$g_{\parallel} = 2.00$, $g_{\perp} = 2.17$, $A_{\parallel} = 11$ G, $A_{\perp} = 92$ G	23, 28

^a From *Paracoccus denitrificans* CcO (see ref 7). ^b All parameters were derived from simulated spectra. ^c ⁶⁵Cu- and [¹⁵N]histidine-enriched N₂OR from *P. stutzeri* (see ref 6). ^d Only ranges were reported for the absorption maxima and molar absorptivities. ^e No esd reported.

with no electronic exchange between the d⁹ and d¹⁰ metal centers.^{12,15} A small number of class II dicopper complexes have been characterized.^{12,16–20} Some exhibit temperature dependent electronic exchange phenomena, whereby the unpaired electron becomes spin-trapped upon cooling, as judged primarily by EPR spectroscopy.^{16–18} Fully delocalized, type III mixed-valence copper complexes which remain delocalized at liquid helium temperatures are rare.

The two types of class III dicopper complexes described to date employ either a tridentate N₂S ligand, LⁱPrdacoS,^{21,22} or octaazacryptand macrobicyclic ligands, L¹–L³ (Table 1).^{23–25} Apart from their different bridging functionalities, the two

ligands afford complexes with very different Cu•••Cu distances and metal ion geometries. The N₂S ligand provides a Cu(1.5)–Cu(1.5) complex of overall C_i symmetry, each Cu having

- (15) Dunaj-Jurco, M.; Ondrejovic, G.; Melnik, M.; Garaj, J. *Coord. Chem. Rev.* **1988**, *83*, 1–28.
 (16) Hendrickson, D. N.; Long, R. C.; Hwang, Y. T.; Chang, H. R. In *Biological and Inorganic Copper Chemistry*; Karlin, K. D., Zubieta, J., Eds.; The Adenine Press: Guilderland, NY, 1984; Vol. 1, pp 223–238.
 (17) Long, R. C.; Hendrickson, D. N. *J. Am. Chem. Soc.* **1983**, *105*, 1513–1521.
 (18) Gagne, R. R.; Koval, C. A.; Smith, T. J.; Cimolino, M. C. *J. Am. Chem. Soc.* **1979**, *101*, 4571–4580.
 (19) Westmoreland, T. D.; Wilcox, D. E.; Baldwin, M. J.; Mims, W. B.; Solomon, E. I. *J. Am. Chem. Soc.* **1989**, *111*, 6106–6123.

- (20) (a) A Cu^ICu^{II} mixed-valence “acetate/methanol” complex has been reported, and support for a delocalized structure at room temperature and at 77 K was acquired by EPR spectroscopy. This complex was never isolated, however, and it disproportionated to a large extent upon cooling below ~–50 °C as judged by the presence of a significant mononuclear Cu(II) impurity in the EPR spectrum. See: Sigwart, C.; Hemmerich, P.; Spence, J. T. *Inorg. Chem.* **1968**, *7*, 2545–2548. (b) In more recent work, the same or a closely related mixed-valence species was generated photochemically or electrochemically from Cu(II) acetate, and the product was characterized by UV–vis and EPR spectroscopy. See: (i) Toledo, I.; Arancibia, M.; Andrade, C.; Crivelli, I. *Polyhedron* **1998**, *17*, 173–178 and (ii) Crivelli, I. G.; Andrade, C. G. *Inorg. Chim. Acta* **1993**, *203*, 115–120.
 (21) (a) Houser, R. P.; Young, V. G., Jr.; Tolman, W. B. *J. Am. Chem. Soc.* **1996**, *118*, 2101–2102. (b) A related dinuclear mixed-valence copper-mercaptoethylamine complex has been prepared and spectroscopically characterized. See: Loeb, B.; Crivelli, I.; Andrade, C. *Inorg. Chim. Acta* **1995**, *231*, 21–27. We restrict our comparative analysis to the LⁱPrdacoS complex described in ref 21a, however, because structural data are available for this compound.
 (22) Abbreviations: LiPrdacoS = 1-isopropyl-5-ethylthiolato-1,5-diazocyclooctane; L¹ = N(CH₂CH₂N=CH–CH=NCH₂CH₂)₃N; L² = N(CH₂CH₂NH–CH₂–CH₂–NHCH₂CH₂)₃N; L³ = N(CH₂CH₂CH₂–N=CH–CH=NCH₂CH₂CH₂)₃N.

distorted trigonal pyramidal geometry. The Cu...Cu distance of 2.9306(9) Å is long and there is presumably no metal–metal bond. Ligands L¹–L³ afford *D*_{3d} symmetric complexes with trigonal bipyramidal Cu centers and Cu–Cu distances of 2.448(1), 2.415(1), and 2.419(1) Å, respectively. The identical coordination environments about the two copper ions within each of the complexes are consistent with delocalized mixed-valence formulations in the solid state. Such delocalization is revealed by their frozen solution EPR (*T* = 4–20 K) and electronic absorption spectral properties, summarized in Table 1. The N₂S-derived complex exhibits a rhombic EPR spectrum with a seven-line hyperfine pattern on the two lower field components arising from spin delocalization over both *I* = 3/2 Cu ions. EPR spectra obtained for complexes with the octaazacryptands are axial and display seven-line hyperfine coupling on the lower field A_{||} component, indicating substantial d_{z²} character in the ground state. The electronic absorption spectra of all the complexes exhibit relatively intense ($\epsilon > 1000 \text{ M}^{-1} \text{ cm}^{-1}$) features in the near-infrared (NIR) region, but the absorption maxima differ substantially for the two different types of complexes, suggesting different electronic structures.

Recently, in two independent studies,^{13,26–28} detailed descriptions of the electronic structures of the Cu_A center and its models were put forth based on thorough analyses of UV–vis, NIR, MCD, EPR, EXAFS, and X-ray structural data, coupled with molecular orbital calculations. The singly occupied molecular orbital (SOMO) for the N₂S-derived mixed-valence complex is partly composed of weakly participating, π -bonding d_{x²-y²} metal orbitals. It is dominated by antibonding sulfur p-orbitals, however, as might have been expected in this case since the Cu atoms are too far apart for direct d-orbital overlap.^{26,27} At the other extreme, in the octaazacryptand systems the σ^* SOMO is composed mainly of d_{z²}-d_{z²} out-of-phase overlap facilitated by the short metal–metal distance and lack of an efficient superexchange pathway through the four-atom bridging groups.²⁶ The σ^* -SOMO for Cu_A was assigned to be a composite of those deduced for these two models, with significant metal d_{x²-y²}-d_{x²-y²} out-of-phase and sulfur p π -p π in-phase overlap.^{26,27} Taken together, these studies suggest that the superexchange pathway in this set of class III mixed-valence complexes comprises overlap between metal d- or ligand p-orbitals, or both, depending on the energetic accessibility of a metal–metal, compared to a bridging, exchange pathway.

The above examples notwithstanding, the paucity of small molecule analogues of the Cu_A center hampers efforts to develop general principles that govern the assembly of dicopper mixed-valence cores and their class III behavior. For example it would be of interest to know (1) what spectrum of ligands will assemble the mixed-valence core and protect it from decomposition pathways such as disproportionation; (2) how the superexchange pathway is affected by Cu–Cu distance, number and donor properties of bridging ligands, metal ion geometries, and the overall complex symmetry; and (3) how these properties

affect the ease with which the mixed-valence core can cycle reversibly between the Cu^ICu^I and Cu(1.5)Cu(1.5) oxidation states with minimal ligand reorganization and at biologically relevant potentials. An efficient approach to exploring these questions is to utilize a readily modified ligand system that will stabilize the Cu(1.5)Cu(1.5) and Cu^ICu^I units, while leaving open coordination sites for docking ancillary ligands with variable donor properties to perturb incrementally the overall electronic structure. This strategy will facilitate the construction of a family of closely related complexes from which the relative importance of the above factors can be evaluated.

In the present investigation, we have approached this goal by using the *m*-xylylenediamine bis(Kemp's triacid imide) (H₂XDK) ligand system,^{29–31} previously demonstrated to be a good platform for binding a variety of metal fragments with labile coordination sites in both bioinorganic^{30,32–39} and organometallic⁴⁰ applications. Previously we described the synthesis and characterization of several bis(carboxylate-bridged) dicopper(I) complexes derived from XDK and π -acceptor and σ -donor ligands.²⁹ In these complexes the copper atoms have linear two-coordinate, trigonal three-coordinate, or pseudo-four-coordinate geometries, and variable Cu–Cu distances ranging from 2.5697(8) to 3.4211(6) Å. Here we report a series of dicopper mixed-valence complexes having variable ancillary ligands which facilitate the analysis of factors that influence their electronic behavior. The synthesis, solid state and solution characterization, and electrochemical behavior of these complexes and related Cu(I) heterometallic complexes are described, the latter serving to enhance our understanding of the electronic properties of the mixed-valence system. A portion of this work was communicated previously.⁴¹

Experimental Section

General Considerations. The complexes [Cu₂(XDK)(MeCN)] (1), [Cu₂(PXDK)(MeCN)] (2), and (Et₃N)[Cu(PXDK)] (3) were prepared according to literature procedures.²⁹ The compound [Fe(OTf)₂(MeCN)₂] was prepared according to a procedure used to obtain the Mn(II) analogue.⁴² All other reagents were procured from commercial sources and used as received unless otherwise noted. THF, benzene, toluene, pentane, and Et₂O were distilled from sodium benzophenone ketyl under nitrogen. Dichloromethane and 1,2-dichloroethane were distilled from CaH₂ under nitrogen. The NMR solvent C₆D₆ was degassed, passed through activated basic alumina, and stored over 3 Å molecular sieves prior to use. All air-sensitive manipulations were carried out either in a nitrogen-filled Vacuum Atmospheres drybox or by standard Schlenk line techniques at room temperature unless otherwise noted.

- (23) Harding, C.; Nelson, J.; Symons, M. C. R.; Wyatt, J. J. *Chem. Soc., Chem. Commun.* **1994**, 2499–2500.
 (24) Harding, C.; McKee, V.; Nelson, J. *J. Am. Chem. Soc.* **1991**, *113*, 9684–9685.
 (25) Barr, M. E.; Smith, P. H.; Antholine, W. E.; Spencer, B. *J. Chem. Soc., Chem. Commun.* **1993**, 1649–1652.
 (26) Farrar, J. A.; Grinter, R.; Neese, F.; Nelson, J.; Thomson, A. J. *J. Chem. Soc., Dalton Trans.* **1997**, 4083–4087.
 (27) Williams, K. R.; Gamelin, D. R.; LaCroix, L. B.; Houser, R. P.; Tolman, W. B.; Mulder, T. C.; deVries, S.; Hedman, B.; Hodgson, K. O.; Solomon, E. I. *J. Am. Chem. Soc.* **1997**, *119*, 613–614.
 (28) Farrar, J. A.; McKee, V.; Al-Obaidi, A. H. R.; McGarvey, J. J.; Nelson, J.; Thomson, A. J. *Inorg. Chem.* **1995**, *34*, 1302–1303.

- (29) LeCloux, D. D.; Lippard, S. J. *Inorg. Chem.* **1997**, *36*, 4035–4046.
 (30) Herold, S.; Lippard, S. J. *J. Am. Chem. Soc.* **1997**, *119*, 145–156.
 (31) Rebeck, J., Jr.; Marshall, L.; Wolak, R.; Parris, K.; Killoran, M.; Askew, B.; Nemeth, D.; Islam, N. *J. Am. Chem. Soc.* **1985**, *107*, 7476–7481.
 (32) Mizoguchi, T. J.; Lippard, S. J. *Inorg. Chem.* **1997**, *36*, 4526–4533.
 (33) Tanase, T.; Yun, J. W.; Lippard, S. J. *Inorg. Chem.* **1996**, *35*, 3585–3594.
 (34) Tanase, T.; Lippard, S. J. *Inorg. Chem.* **1995**, *34*, 4682–4690.
 (35) Yun, J. W.; Tanase, T.; Pence, L. E.; Lippard, S. J. *J. Am. Chem. Soc.* **1995**, *117*, 4407–4408.
 (36) Tanase, T.; Yun, J. W.; Lippard, S. J. *Inorg. Chem.* **1995**, *34*, 4220–4229.
 (37) Watton, S. P.; Masschelein, A.; Rebeck, J., Jr.; Lippard, S. J. *J. Am. Chem. Soc.* **1994**, *116*, 5196–5205.
 (38) Goldberg, D. P.; Watton, S. P.; Masschelein, A.; Wimmer, L.; Lippard, S. J. *J. Am. Chem. Soc.* **1993**, *115*, 5346–5347.
 (39) Hagen, K. S.; Lachicotte, R.; Kitaygorodskiy, A.; Elbouadili, A. *Angew. Chem., Int. Ed. Engl.* **1993**, *32*, 1321–1324.
 (40) Steinhuebel, D. P.; Fuhrmann, P.; Lippard, S. J. *Inorg. Chim. Acta* **1998**, *270*, 527–536.
 (41) LeCloux, D. D.; Davydov, R.; Lippard, S. J. *J. Am. Chem. Soc.* **1998**, *120*, 6810–6811.
 (42) Bryan, P. S.; Dabrowiak, J. C. *Inorg. Chem.* **1975**, *14*, 296–299.

Physical Measurements. NMR spectra were recorded on a Bruker AC-250 or Varian XL-300 spectrometer. ¹H NMR chemical shifts are reported versus tetramethylsilane and referenced to the residual solvent peak. FTIR spectra were recorded on a Bio-Rad FTS-135 FTIR spectrometer. UV–vis–NIR spectra were recorded on a Cary 5E reference spectrophotometer. Conductivity measurements were carried out in THF or CH₂Cl₂ at 296 K with a Fisher Scientific conductivity bridge, model 9-326, outfitted with a platinum black electrode.

Electrochemistry. Cyclic voltammetric measurements were carried out in a Vacuum Atmospheres drybox under N₂ with an EG&G model 263 potentiostat. A three electrode configuration was used consisting of a 1.75 mm² platinum working electrode, a Ag/AgNO₃ (0.1 M in MeCN) reference electrode, and a coiled platinum wire auxiliary electrode. A 0.5 M solution of Bu₄N(PF₆), triply recrystallized from acetone, was used as supporting electrolyte. Solute samples were typically 1–2 mM. Scan rate profiles were conducted for each sample, at scan speeds of 50–500 mV/s, and compared to that obtained for Cp₂Fe under identical conditions. All cyclic voltammograms were externally referenced to Cp₂Fe, for which E_{1/2} = +143 mV in THF (ΔE_p = 68 mV, scan rate = 50 mV/s).

EPR Spectroscopy. For measurements at 9 K, data were collected on a Bruker model 300 ESP X-band spectrometer operating at 9.47 GHz. For measurements at 77 K, data were collected on a Varian E104 X-band spectrometer operating at 9.14 GHz. The Q-band measurements were performed at 2K with a modified Varian E109 spectrometer operating at 35 GHz. Liquid helium temperatures were maintained with an Oxford Instruments EPR 900 cryostat, and liquid nitrogen temperatures with an EPR finger dewar. For all measurements, 1 mM frozen solutions were prepared in 2-methyltetrahydrofuran (2-Me-THF), a solvent in which the samples glassed well. Solid samples (~1 mg) were prepared as finely ground powders. Simulations were carried out with the WINEPR SimFonia program package.⁴³ The fits incorporated coupling of the unpaired spin simultaneously to each I = 3/2 copper center.

Extended Hückel Molecular Orbital Calculations. These computations⁴⁴ were carried out with the program YAeHMOP,⁴⁵ operating on a Silicon Graphics Indy computer. Simplified models of the mixed-valence complexes **7** and **8** were implemented, [Cu₂(μ-O₂CCH₃)₂(OMe₂)₄]⁺ and [Cu₂(OH)₂(OH₂)₂(OMe₂)₄]⁺, and used the core crystallographic coordinates determined for **8**.

Preparation of Compounds. [Cu₂(XDK)(μ-OTf)(THF)₂] (**4**). To a stirred solution of **1** (300 mg, 0.402 mmol) in THF (5 mL) was added a solution of AgOTf (105 mg, 0.402 mmol) in THF (1 mL) in one portion. The colorless solution immediately turned dark purple and an off-white precipitate formed. The mixture was filtered through Celite, and the filtrate was evaporated to dryness. Recrystallization from THF/pentane at –30 °C provided **4** as thin purple blocks which appeared suitable for X-ray crystallography (386 mg, 96%). IR (KBr) 2962, 2935, 2875, 1734, 1691, 1460, 1362, 1297, 1264, 1182, 1024, 868, 760, 637 cm⁻¹; UV–vis (THF, λ_{max}, nm (ε, M⁻¹ cm⁻¹)) 542 (1200), 768 (sh, 300), 956 (630). Anal. Calcd for C₄₅H₆₂N₂O₁₄Cu₂F₃S (**4**·1THF): C, 50.46; H, 5.83; N, 2.62. Found: C, 50.45; H, 6.08; N, 2.47.

[Cu₂(PXDK)(μ-OTf)(THF)₂] (**5**). **Method A.** This compound was prepared from **2** (50 mg, 0.055 mmol) and AgOTf (14 mg, 0.055 mmol) by an analogous procedure to that used to prepare **4**. Recrystallization from pentane and a trace amount of THF at –30 °C afforded **5** as purple needles (29 mg, 45%).

Method B. To a stirred suspension of **3** (50 mg, 0.053 mmol) in THF (2 mL) was added Cu(OTf)₂ (19.6 mg, 0.053 mmol) in THF (1 mL) in one portion. Complex **3** was immediately consumed and the solution turned dark purple. After 15 min the THF was removed in vacuo. The solid residue was taken up in Et₂O (2–3 mL) and then filtered through Celite to remove the precipitated Et₄N(OTf). Solvent removal in vacuo followed by recrystallization provided **5** as purple needles. (25 mg, 40%). IR (KBr) 2962, 2935, 2875, 1733, 1691, 1534,

1460, 1362, 1296, 1182, 1024, 868, 637 cm⁻¹. Anal. Calcd for C₅₃H₇₈N₂O₁₃Cu₂F₃S: C, 54.53; H, 6.73; N, 2.40. Found: C, 54.34; H, 6.54; N, 2.61.

[Cu₂(XDK)(μ-O₂CCF₃)(THF)₂] (**6**). This compound was prepared from **1** (150 mg, 0.201 mmol) and AgO₂CCF₃ (44 mg, 0.20 mmol) by an analogous procedure to that used to prepare **4**. Recrystallization from THF/pentane provided **6** as purple blocks which appeared suitable for X-ray crystallography (152 mg, 79%). IR (KBr) 2980, 2933, 2878, 1734, 1695, 1662, 1500, 1467, 1421, 1381, 1353, 1336, 1230, 1183, 1141, 1035, 838, 761, 667, 477 cm⁻¹; UV–vis (THF, λ_{max}, nm (ε, M⁻¹ cm⁻¹)) 563 (2000), 806 (sh, 320), 942 (sh, 360), 1250 (500). Anal. Calcd for C₄₂H₅₄N₂O₁₂Cu₂F₃: C, 52.39; H, 5.65; N, 2.91. Found: C, 52.17; H, 5.63; N, 2.89.

[Cu₂(XDK)(THF)₄](BF₄) (**7**). This compound was prepared from **1** (100 mg, 0.134 mmol) and AgBF₄ (26 mg, 0.13 mmol) by an analogous procedure to that used to prepare **4**. Recrystallization from THF/pentane provided **7** as purple plates (120 mg, 82%). IR (KBr) 2969, 2927, 2875, 1734, 1698, 1540, 1462, 1423, 1353, 1230, 1028, 957, 864, 759, 676, 523 cm⁻¹; UV–vis (THF, λ_{max}, nm (ε, M⁻¹ cm⁻¹)) 536 (1600), 923 (1200). Anal. Calcd for C₄₈H₇₀N₂O₁₂Cu₂BF₄: C, 51.29; H, 5.81; N, 2.99. Found: C, 50.98; H, 5.92; N, 3.04.

[Cu₂(PXDK)(THF)₄](BF₄) (**8**). This compound was prepared from **2** (121 mg, 0.132 mmol) and AgBF₄ (26 mg, 0.132 mmol) by an analogous procedure to that used to prepare **4**. Recrystallization from THF/pentane provided **8** as purple needles which appeared suitable for X-ray crystallography (101 mg, 61%). IR (KBr) 2962, 2933, 2869, 1734, 1692, 1540, 1459, 1362, 1314, 1264, 1182, 1034, 866, 759, 673, 586 cm⁻¹; UV–vis (THF, λ_{max}, nm (ε, M⁻¹ cm⁻¹)) 527 (1700), 878 (1200). Anal. Calcd for C₆₀H₉₄N₂O₁₂Cu₂BF₄: C, 57.68; H, 7.58; N, 2.24. Found: C, 56.84; H, 7.25; N, 2.42.

[CuZn(PXDK)(OTf)(THF)₂(H₂O)] (**9**). This compound was prepared from **3** (200 mg, 0.213 mmol) and Zn(OTf)₂ (94 mg, 0.21 mmol) by a procedure analogous to method B used to prepare **5**, except that the reaction mixture was allowed to stir for 12 h. Recrystallization from pentane with a trace of THF provided **9** as colorless blocks which appeared suitable for X-ray crystallography (154 mg, 61%). ¹H NMR (300 MHz, C₆D₆, 296 K) δ 7.31 (1H, s), 6.63 (1H, s), 3.83 (8H, br s), 2.90–2.60 (4H, m), 2.30–1.92 (6H), 1.83 (6H, s), 1.68–1.03 (34H, m), 1.03–0.80 (16H, m), 0.75 (4H, d, J = 12.6 Hz); IR (KBr) 3451, 2963, 2933, 2874, 1734, 1676, 1577, 1459, 1365, 1309, 1184, 1027, 918, 761, 637 cm⁻¹. Anal. Calcd for C₅₃H₈₀N₂O₁₄CuZnF₃S: C, 53.62; H, 6.79; N, 2.36. Found: C, 54.22; H, 6.55; N, 2.34.

[CuFe(PXDK)(OTf)(NB)(MeCN)]₂ (**10**). To a stirred suspension of **3** (200 mg, 0.213 mmol) in THF (3 mL) was added [Fe(OTf)₂(MeCN)₂] (106 mg, 0.243 mmol) in THF (1 mL) in one portion. After 15 min the THF was removed in vacuo. The solid residue was taken up in Et₂O (2–3 mL) and then filtered through Celite. Solvent removal in vacuo followed by recrystallization from 1,2-dichloroethane/norbornene (NB, 1:1, v/v) and pentane afforded **10** as small colorless blocks (146 mg, 60%) which appeared suitable for X-ray crystallography. IR (KBr) 3049, 2871, 2742, 1737, 1699, 1594, 1502, 1412, 1368, 1315, 1181, 1033, 926, 862, 762, 637 cm⁻¹. Anal. Calcd for C₅₄H₇₅N₃O₁₁CuFeF₃S: C, 56.47; H, 6.57; N, 3.65. Found: C, 55.58; H, 6.80; N, 3.38. This sample was heated in vacuo at 90 °C for 6 h in an attempt to remove completely the two lattice dichloroethane molecules, which were identified by X-ray crystallography. Apparently only partial elimination was achieved, and subsequent heating at higher temperatures resulted in decomposition of the complex.

[CuZn(PXDK)(OTf)(NB)(H₂O)] (**11**). Compound **9** was prepared in situ from **3** (38 mg, 0.040 mmol) and Zn(OTf)₂ (15 mg, 0.040 mmol) and then recrystallized from benzene/norbornene (1:1, v/v) and pentane to afford **11** as colorless blocks, which appeared suitable for X-ray crystallography (27 mg, 57%). ¹H NMR (250 MHz, C₆D₆, 296 K) δ 7.35 (1H, s), 6.61 (1H, s), 5.22 (2H, s), 3.82 (4H, br s), 2.95–2.72 (6H, m), 2.30–1.90 (8H, m), 1.79 (6H, s), 1.68–0.60 (46H, m); IR (KBr) 3314, 2964, 2933, 2875, 1737, 1682, 1603, 1505, 1459, 1410, 1367, 1334, 1236, 1201, 1018, 926, 762, 637 cm⁻¹. Anal. Calcd for C₅₂H₇₄N₂O₁₂CuZnF₃S: C, 54.92; H, 6.55; N, 2.46. Found: C, 55.63; H, 6.78; N, 2.42.

Collection and Reduction of X-ray Data. All crystals were mounted on the tips of glass fibers with Paratone N (Exxon), cooled to low

(43) WINEPR-SimFonia, 1.25; Bruker Analytik GmbH: Karlsruhe, FRG, 1994–1996.

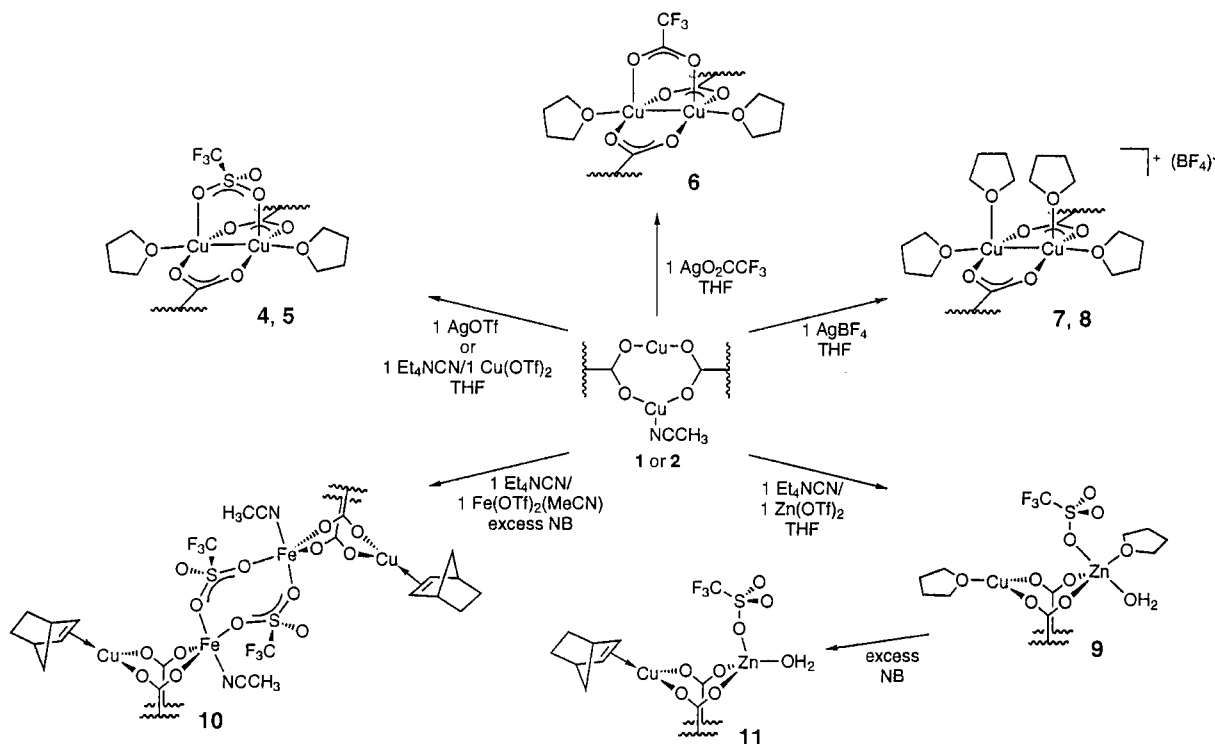
(44) Hoffmann, R. *J. Chem. Phys.* **1963**, *39*, 1397–1412.

(45) Landrum, G. A. *YAeHMOP: Yet Another extended Hückel Molecular Orbital Package*, 2.0; Cornell University: Ithaca, NY, 1995.

Table 2. Summary of X-ray Crystallographic Data

	4·2THF	6·0.5THF	8·1THF	9·0.5THF	11
formula	C ₄₉ H ₇₀ N ₂ O ₁₅	C ₄₄ H ₅₈ N ₂ O _{12.5}	C ₆₄ H ₁₀₂ N ₂ O ₁₃	C ₅₅ H ₈₄ N ₂ O _{14.5}	C ₅₂ H ₇₄ N ₂ O ₁₂
fw	1143.21	4977.49	1321.37	1223.21	1137.10
space group	<i>P</i> 2 ₁ / <i>n</i>	<i>P</i> 2 ₁ 2 ₁	<i>P</i> 2 ₁ / <i>n</i>	<i>C</i> 2/ <i>c</i>	<i>P</i> 2 ₁ / <i>n</i>
<i>a</i> , Å	20.203(2)	11.02460(10)	17.4237(9)	25.0154(5)	15.5186(2)
<i>b</i> , Å	12.0901(10)	16.31380(10)	21.5206(12)	18.2877(2)	24.28620(10)
<i>c</i> , Å	22.130(2)	27.67530(10)	18.8570(10)	25.9855(5)	15.93940(10)
β , deg	94.522(5)		105.9970(10)	92.1000(10)	113.3850(10)
<i>V</i> , Å ³	5388.6(8)	4977.49(6)	6797.0(6)	11879.7(4)	5513.91(8)
<i>Z</i>	4	4	4	4	2
ρ_{calcd} , g/cm ³	1.409	1.333	1.291	1.368	1.370
<i>T</i> , °C	-85	-85	-85	-85	-85
μ (Mo K α), mm ⁻¹	0.904	0.924	0.696	0.870	0.929
transmission coeff	0.817–1.000	0.668–1.000	0.806–1.000	0.885–1.000	0.718–1.000
2 θ limits, deg	3–46	3–46	3–46	3–57	3–57
total no. of data	20 000	19 795	25 459	33 683	31 387
no. of unique data	7456	7086	9533	13 213	12 392
no. of observed data ^a	5684	6246	6996	8258	7881
no. of parameters	624	559	748	686	704
<i>R</i> (%) ^b	5.19	4.71	8.50	6.75	7.09
wR2 (%) ^c	12.59	12.45	18.14	16.37	17.60
max, min peaks, e/Å ³	0.533, -0.378	0.744, -0.380	1.112, -0.448	0.984, -0.613	0.792, -0.753

^a Observation criterion: $I > 2\sigma(I)$. ^b $R = \sum ||F_o| - |F_c|| / \sum |F_o|$. ^c $wR2 = \{\sum [w(F_o^2 - F_c^2)^2] / \sum [w(F_o^2)^2]\}^{1/2}$.

Scheme 1

temperature (~ -85 °C), and placed on a Siemens CCD X-ray diffraction system controlled by a Pentium-based PC running the SMART software package.⁴⁶ The general procedures for data collection and reduction follow those reported previously.⁴⁷ All structures were solved with the direct methods programs SIR-92⁴⁸ or XS, part of the TEXSAN⁴⁹ and SHELXTL⁵⁰ program packages, respectively. Structure

refinements were carried out with XL, part of the SHELXTL program package.⁵⁰ All non-hydrogen atoms were located and their positions refined by a series of least-squares cycles and Fourier syntheses. Hydrogen atoms were assigned idealized positions and given a thermal parameter 1.2 times the thermal parameter of the carbon atom to which each was attached. Empirical absorption corrections were calculated and applied for each structure by using SADABS, part of the SHELXTL program package.⁵⁰

In the structure of **4**, each coordinated THF molecule as well as one of the two lattice THF molecules contain a carbon atom disordered over two positions. In each case the atom was distributed over two positions and refined. In the structure of **6** each coordinated THF molecule was disordered over two positions. In one molecule, two of the carbon atoms and the oxygen atom were refined at full occupancy, and the occupancy of the remaining two carbon atoms was distributed

(46) SMART, 4.0; Siemens Industrial Automation, Inc.: Madison, WI, 1994.

(47) Feig, A. L.; Bautista, M. T.; Lippard, S. J. *Inorg. Chem.* **1996**, *35*, 5, 6892–6898.

(48) Burla, M. C.; Camalli, M.; Cascarano, G.; Giacovazzo, C.; Polidori, G.; Spagna, R.; Viterbo, D. *J. Appl. Crystallogr.* **1989**, *22*, 389–393.

(49) TEXSAN: Single-Crystal Structure Analysis Software, 1.6c; Molecular Structure Corporation: The Woodlands, TX, 1995.

(50) SHELXTL: Structure Analysis Program, 5.0; Siemens Industrial Automation, Inc.: Madison, WI, 1995.

Table 3. Selected Bond Distances and Angles^a

		distance (Å)	angle (deg)	
4	Cu1–Cu2	2.4093(8)	O102–Cu1–O202	164.6(2)
	Cu1–O102	1.873(3)	O102–Cu1–O401	96.4(2)
	Cu1–O202	1.873(3)	O401–Cu1–O502	98.28(3)
	Cu1–O401	2.315(4)	O101–Cu2–O201	164.03(14)
	Cu1–O502	2.060(3)	O101–Cu2–O402	100.26(14)
	Cu2–O101	1.891(3)	O402–Cu2–O501	91.82(13)
	Cu2–O201	1.887(3)	Cu1–Cu2–O402	92.27(10)
	Cu2–O402	2.242(3)	Cu2–Cu1–O401	87.94(10)
	Cu2–O501	2.052(3)		
	6	Cu1–Cu2	2.3988(8)	O102–Cu1–O202
Cu1–O102		1.910(4)	O102–Cu1–O401	99.9(2)
Cu1–O202		1.908(4)	O401–Cu1–O502	97.5(2)
Cu1–O401		2.150(4)	O101–Cu2–O201	156.6(2)
Cu1–O502		2.050(4)	O101–Cu2–O402	105.8(2)
Cu2–O101		1.891(3)	O402–Cu2–O501	97.7(2)
Cu2–O201		1.889(3)	Cu1–Cu2–O402	87.03(12)
Cu2–O402		2.166(4)	Cu2–Cu1–O401	88.27(13)
Cu2–O501		2.083(3)		
8		Cu1–Cu2	2.4246(12)	O102–Cu1–O202
	Cu1–O102	1.885(4)	O102–Cu1–O401	102.6(2)
	Cu1–O202	1.883(4)	O401–Cu1–O402	89.6(2)
	Cu1–O401	2.285(5)	O101–Cu2–O201	166.3(2)
	Cu1–O402	2.087(5)	O101–Cu2–O501	91.8(2)
	Cu2–O101	1.883(5)	O501–Cu2–O502	90.3(2)
	Cu2–O201	1.881(5)	Cu1–Cu2–O501	101.26(14)
	Cu2–O501	2.270(5)	Cu2–Cu1–O401	102.7(2)
	Cu2–O502	2.042(5)		
	9	Cu1···Zn1	2.8810(8)	O102–Cu1–O202
Cu1–O102		1.891(3)	O102–Cu1–O401	102.40(12)
Cu1–O202		1.890(3)	O202–Cu1–O401	93.52(13)
Cu1–O401		2.228(3)	O101–Zn1–O201	150.03(13)
Zn1–O101		1.930(3)	O101–Zn1–O501	92.71(14)
Zn1–O201		1.938(3)	O501–Zn1–O504	90.45(14)
Zn1–O501		2.145(3)	O501–Zn1–O505	178.64(13)
Zn1–O504		2.025(3)		
Zn1–O505		2.189(3)		
11		Cu1···Zn1	3.732(2)	O102–Cu1–O202
	Cu1'···Zn1	3.294(2)	O102–Cu1'–O202	107.0(2)
	Cu1–O102	1.981(3)	O102–Cu1–C401	104.3(4)
	Cu1–O202	1.973(3)	O102–Cu1'–C41	105.2(4)
	Cu1–C401	2.044(14)	O101–Zn1–O201	132.26(13)
	Cu1–C402	2.12(2)	O101–Zn1–O501	99.57(14)
	Cu1'–O102	1.998(3)	O101–Zn1–O504	103.15(12)
	Cu1'–O202	2.027(3)	O201–Zn1–O501	106.85(14)
	Cu1'–C41	2.024(12)	O201–Zn1–O504	105.59(12)
	Cu1'–C42	2.004(11)		
	Zn1–O101	1.911(3)		
	Zn1–O201	1.917(3)		
	Zn1–O501	2.021(3)		
	Zn1–O504	1.970(3)		

^a Numbers in parentheses are estimated standard deviations of the last significant figure. Atoms are labeled as indicated in Figures 2 and 3.

over two positions and refined. In the other, the occupancy of one carbon atom was distributed over two positions and refined, and the remaining atoms were refined at full occupancy. The lattice THF molecule in **6** contains large thermal parameters, so each atom was refined at a site occupancy of 0.5. Two of the coordinated THF molecules in the structure of **8** were disordered over two positions. Two of the carbon atoms and the oxygen atom were refined at full occupancy, whereas the remaining carbon atoms were distributed over two positions and refined. The structure of **9** contains a coordinated THF molecule disordered over two positions, and it was refined in a fashion similar to that described for the structure of **4**. Finally, in the structure of **11** the copper atom and norbornene ligand are disordered. The site occupancy of this fragment was distributed over two positions and refined. Bond distances and angles for each orientation of **11** are reported in Table 3. For both structures **9** and **11**, the assignment of the metal atom positions as Cu or Zn was based on chemically

reasonable presumptions that (a) the overall neutral charge of each complex necessitates the assignment of one mono- and one divalent metal ion; (b) the three-coordinate geometry for the metal coordinated to the norbornene ligand in **11** is quite common for Cu(I) but not for Zn(II); and (c) the Cu–C distances in **11** are nearly identical to those observed for [Cu₂(XDK)(NB)₂].²⁹

Important crystallographic information for each complex, including refinement residuals, is available in Table 2. Selected bond distances and angles for the coordination spheres of each structurally characterized complex are displayed in Table 3. Final positional, equivalent isotropic thermal, and anisotropic temperature parameters, as well as all bond distances and angles, are provided as CIF files in Tables S1–S10 of the Supporting Information for complexes **10** and **11**, or in ref 40 for **4**, **6**, and **8**.

Results and Discussion

Preparation and Structural Characterization of Mixed-Valence Complexes [Cu₂(XDK)(μ-OTf)(THF)₂] (4**), [Cu₂(PXDK)(μ-OTf)(THF)₂] (**5**), [Cu₂(XDK)(μ-O₂CCF₃)(THF)₂] (**6**), [Cu₂(XDK)(THF)₄](BF₄) (**7**), and [Cu₂(PXDK)(THF)₄](BF₄) (**8**).** Each of these complexes was prepared by one-electron oxidation of acetonitrile adducts **1** or **2** with the appropriate silver(I) salt in THF (Scheme 1). Removal of the resulting solids followed by recrystallization afforded **4–8** as deep purple compounds in moderate to excellent yield. Recovery of **5** and **8** was limited by their significant solubility under the recrystallization conditions. The products appeared to be stable in the presence of excess Ag⁺, suggesting that these mixed-valence complexes are resistant to disproportionation followed by further Ag⁺ oxidation of the remaining equivalent of Cu(I). By contrast, oxidation of **1** or **2** with Ag⁺ salts of more basic anions, such as benzoate, led to mixtures of intractable blue-green products. This result indicates that ancillary ligands more donating than trifluoroacetate are incompatible with the mixed-valence dicopper–XDK framework. The triflate adduct **5** could also be prepared from mononuclear PXDK complex **3** and Cu(OTf)₂. Because of the propyl groups in PXDK, **5** is readily soluble in Et₂O, allowing the Et₄N(OTf) byproduct to be removed conveniently by filtration.

The IR spectra of compounds **4–8** display new features attributable to their respective anions. In addition, the XDK carboxylate stretch in the dicopper(I) starting materials **1** and **2** is shifted by 5–15 cm⁻¹ to lower energy for each product, indicating a change in Cu geometry. The UV–vis spectra of the products exhibit a relatively sharp and intense (ε = 1200–2000 M⁻¹ cm⁻¹) feature with a maximum at ~545 nm (Figure 1). For the three XDK complexes, this band is most intense for the trifluoroacetate derivative. In the visible/near-infrared region, all the complexes show broad absorptions between 700 and 1500 nm. On the basis of the peak shapes, this feature appears to arise from a single transition for the BF₄⁻ complexes, but is made up of overlapping components for the OTf⁻ and O₂CCF₃⁻ adducts. A similarly intense (ε > 500 M⁻¹ cm⁻¹) feature at low energy has been observed in other class II and III mixed-valence copper complexes. In the class II systems it was assigned as an intervalence charge transfer^{17,18} and, in the class III complexes, as a ψ → ψ* transition within the Cu(1.5)Cu(1.5) manifold.^{13,26} The relatively sharp transition observed for the BF₄⁻ adduct parallels those observed for the class III octaaza-cryptand complexes,^{25,26} but the multiple bands appearing in the spectra of the triflate and trifluoroacetate derivatives are currently not understood. In the absence of additional information such as MCD or single-crystal data, we choose neither to assign the NIR transitions nor to make a definitive class II or III designation based on these spectra.

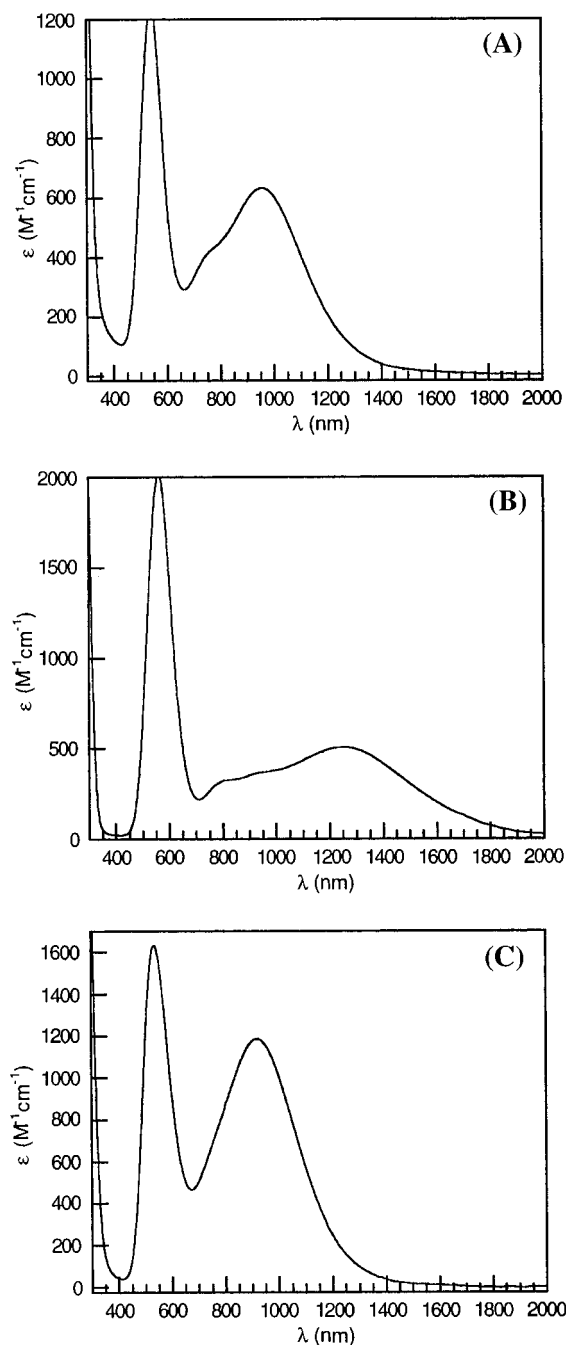


Figure 1. Electronic absorption spectra of (A) $[\text{Cu}_2(\text{XDK})(\mu\text{-OTf})(\text{THF})_2]$ (**4**), 0.74 mM in THF; (B) $[\text{Cu}_2(\text{XDK})(\mu\text{-O}_2\text{CCF}_3)(\text{THF})_2]$ (**6**), 0.74 mM in THF; and (C) $[\text{Cu}_2(\text{XDK})(\text{THF})_4](\text{BF}_4)$ (**7**), 0.47 mM in THF.

The solution stability of the mixed-valence complexes was assessed by UV-vis spectroscopic and conductivity measurements. In all cases, the optical spectra remained unchanged after standing in THF, benzene, or CH_2Cl_2 for several days under N_2 . Upon addition of a strongly coordinating solvent such as MeCN, however, the solutions immediately turned pale blue-green and absorption spectra typical of mononuclear Cu(II) were observed. The conductivity behavior of **4–8** similarly remained unchanged over the same time period in THF solution. The triflate and O_2CCF_3^- adducts are nonelectrolytes, whereas the BF_4^- adducts are 1:1 electrolytes as judged by a comparison of conductivity vs concentration plots for **7** and $\text{Bu}_4\text{N}(\text{PF}_6)$ (Supporting Information). These results demonstrate that the $\{\text{Cu}_2(\text{XDK})\}^+$ mixed-valence core is highly resistant to dis-

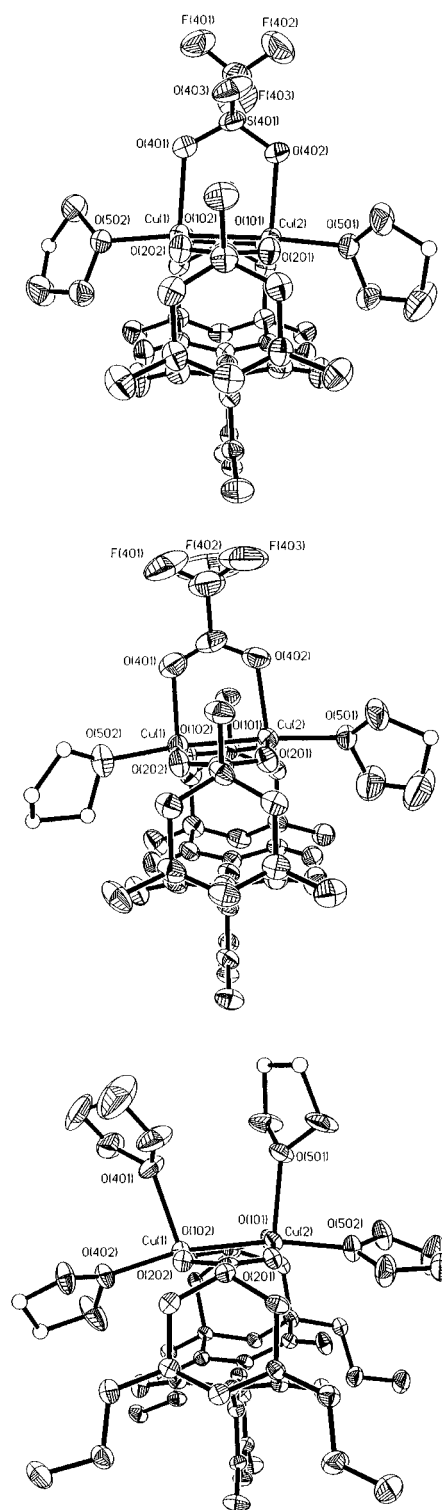


Figure 2. ORTEP diagrams with 50% thermal ellipsoids (top to bottom) of $[\text{Cu}_2(\text{XDK})(\mu\text{-OTf})(\text{THF})_2]$ (**4**), $[\text{Cu}_2(\text{XDK})(\mu\text{-O}_2\text{CCF}_3)(\text{THF})_2]$ (**6**), and $[\text{Cu}_2(\text{PXDK})(\text{THF})_4](\text{BF}_4)$ (**8**).

proportionation, even in the absence of excess THF, provided only weak field ligands are present.

The structures of **4**, **6**, and **8**, as determined by X-ray crystallography, are displayed in Figure 2. Selected bond distances and angles are listed in Table 3. The structure of the triflate adduct **4** consists of two slightly distorted square pyramidal copper atoms, each ligated by two XDK carboxylate oxygens, a THF molecule, and an oxygen atom of a bridging triflate ion. The bond distances and angles about each Cu atom

are almost identical, and the dinuclear complex has idealized C_{2v} geometry, although no symmetry is crystallographically imposed on the molecule. Both copper atoms are situated slightly above (0.241(2) Å) the rigidly disposed and coplanar XDK carboxylate oxygen atoms, with nearly identical O_{XDK} –Cu– O_{XDK} angles. The fifth coordination site is filled by the adjacent copper fragment, the Cu–Cu distance being 2.4093(8) Å. This value is significantly smaller than the 2.6287(5) Å distance in the dicopper(I) in starting material **1** or in homoleptic $Cu_2(XDK)$, where the average Cu···Cu distance is 2.5901(9) Å.²⁹ The Cu–Cu bond in **4** is on the order of that observed for the octaazacryptand class III mixed-valence complexes (Table 1).²⁸ The longest Cu–O distance is that to the triflate oxygen atom, which is ~0.2 Å longer than the Cu–O bond involving THF, which identifies the triflate as the axial ligand of the square pyramid. Because the ligand fields presented by the three different type donor atoms, the carboxylates, THF and copper, differ widely, the true symmetry at each metal center is rhombic, as reflected by EPR spectroscopy (vide infra).

The solid-state structure for trifluoroacetate analogue **6** is quite similar to that of **4**, with a few important distinctions. First, the Cu–Cu bond in **6** is 2.3988(8) Å, the shortest distance thus far observed for dicopper-XDK complex. Second, the axial Cu–O bonds to the trifluoroacetate ligand have shortened by ~0.1 Å. Third, the O_{XDK} –Cu– O_{XDK} angles have contracted by ~10°, reflecting displacement of the copper atoms by 0.363(3) Å from the plane of the XDK carboxylate oxygen atoms. In addition, the Cu– O_{XDK} bond lengths are slightly longer in **6** versus **4**. All of these differences reflect the superior donor properties of the trifluoroacetate ligand compared to triflate, their relative pK_a values being 0.3⁵¹ and –5.9,⁵² respectively. Trifluoroacetate provides a greater share of the overall electron density required by each copper ion, diminishing the bonding interaction to the XDK carboxylate oxygens in **6**. Overall the tris(carboxylate-bridged) motif comprises a superior set of bridging ligands, however, a feature which accounts for the slightly shorter Cu–Cu distance in **6** compared to **4**.

In the structure of **8**, the bridging anion has been displaced in favor of THF ligands, due to the poor donor properties of the BF_4^- anion and its even rarer tendency to serve as a bridging ligand. Without the third bridge, the Cu–Cu distance in **8** has lengthened slightly compared to that in **4**. The axial Cu– O_{THF} bond lengths and the O_{XDK} –Cu– O_{XDK} angles are quite similar to the analogous values in **4**, however.

Preparation and Structural Characterization of Heterodimetallic Complexes [CuZn(PXDK)(OTf)(THF)₂(H₂O)] (9**), [CuFe(PXDK)(OTf)(NB)(MeCN)₂] (**10**), and [CuZn(PXDK)(OTf)(NB)(H₂O)] (**11**).** Heterodimetallic complexes containing Cu(I) and divalent non-copper ions were sought to help delineate the significance of metal–metal bonding in the dicopper mixed-valence derivatives. If the close contact between copper atoms in the latter were only a consequence of the bridging XDK ligand, then a similar metal–metal distance might be expected for analogous $Cu^I M^{II}(\mu-XDK)$ complexes. It is difficult to duplicate exactly the ligand composition of the Cu(II) fragment in **4**–**8**, which would render such a comparison most relevant. The successful preparation of triflate complex **5** from mononuclear **3** and $Cu(OTf)_2$ by Method B (Experimental Section), however, suggested a route to the desired mixed-metal complexes by substituting $M(OTf)_2$ starting materials for copper(II) triflate under identical reaction conditions.

Exposure of **3** to a suspension of $Zn(OTf)_2$ in THF resulted in gradual consumption of both reagents over 12 h (Scheme 1). As was the case for **5**, the purification of $Cu^I Zn^{II}$ complex **9** was facilitated by its solubility in ether, which allowed insoluble $Et_4N(OTf)$ to be filtered off. The analogous reaction with the XDK analogue of **3** yielded an identical product, as judged by ¹H NMR spectroscopy, but it could not be separated from a trace amount of water in the $Zn(OTf)_2$ reagent or in the ethereal solvents; the synthesis proved to be quite reproducible, however.

The ¹H NMR spectrum of **9** displays a single set of XDK and THF resonances in a 1:1 ratio. Some of the upfield XDK resonances corresponding to protons adjacent to the metal binding sites, and the two THF resonances, were broadened at room temperature. We ascribe this behavior to dynamic exchange involving the THF ligand. A resonance that could be assigned to water was presumably obscured by the ligand resonances, but the identity of this ligand was confirmed by X-ray crystallography, elemental analysis, and IR spectroscopy.

Complex **10** was prepared from **3** and $[Fe(OTf)_2(MeCN)_2]$ in a similar fashion. The THF complex analogous to **9** did not afford crystalline material until excess norbornene was added, which presumably displaces the THF ligand bound to copper(I) in the precursor complex. A similar transformation was accomplished with the $Cu^I Zn^{II}$ complex by recrystallizing it in the presence of excess norbornene to provide **11**. Triflate complex **4** was unreactive toward excess norbornene under similar conditions, as judged by UV–vis spectroscopy. This result suggests that delocalization in this complex may mask any reactivity as a copper(I) species, and that a Cu(1.5)Cu(1.5) oxidation state assignment is more appropriate for **4**–**8**. Alternatively, kinetic factors may explain the inertness of **4** toward norbornene.

The solid-state structures of **9** and **11** are presented in Figure 3. The structure of **9** consists of a trigonal copper atom ligated by a THF and two carboxylate oxygen atoms. The zinc atom is trigonal bipyramidally coordinated by five oxygen atoms contributed by two from PXDK, a monodentate, terminal triflate, a THF, and a water molecule. The water is hydrogen bonded to the imide carbonyls of the PXDK ligand, a common feature in XDK complexes when water or alcohol ligands are present.^{33–35,37} The triflate ligand displays no affinity for Cu(I), and the metal–metal distance in this complex has lengthened to 2.8810(8) Å, compared to 2.4093(8) Å for the triflate analogue **4**. The X-ray structure of **11** is somewhat analogous to that determined for **9** in that the copper atom is trigonal, the triflate ligand is coordinated in the same fashion, and the metal ions are well separated from one another. The copper–norbornene fragment is disordered over two positions with equal site occupancies in each orientation. These two binding modes were also observed within the same molecule of $[Cu_2(XDK)(NB)_2]$,²⁹ and are judged to be energetically similar.

The structure of **10** was of only modest quality,⁵³ but it served to identify the overall geometry and is depicted in Scheme 1. The complex dimerizes in the solid state via bridging triflate groups, the two halves of the dimer being related by a center of inversion. Qualitatively, the Cu···Fe separation of 3.492(2) Å is similar to the Cu···Zn distances in **11**. Thus replacement

(51) *The Merck Index*, 12th ed.; Budavari, S., Ed.; Merck Research Laboratories: Whitehouse Station, NJ, 1996.

(52) Guthrie, J. P. *Can. J. Chem.* **1978**, *56*, 2342–2354.

(53) X-ray data for **10** from dichloroethane/pentane: $P2/n$, $a = 19.0883(5)$ Å, $b = 14.5289(3)$ Å, $c = 23.4342(6)$ Å, $\beta = 109.1900(10)^\circ$, $V = 6137.9(3)$ Å³, $Z = 4$, $T = 188$ K, $R = 14.12\%$, $wR2 = 40.36$. This structure was not fully refined due to major disorder of the two dichloroethane molecules in the crystal lattice.

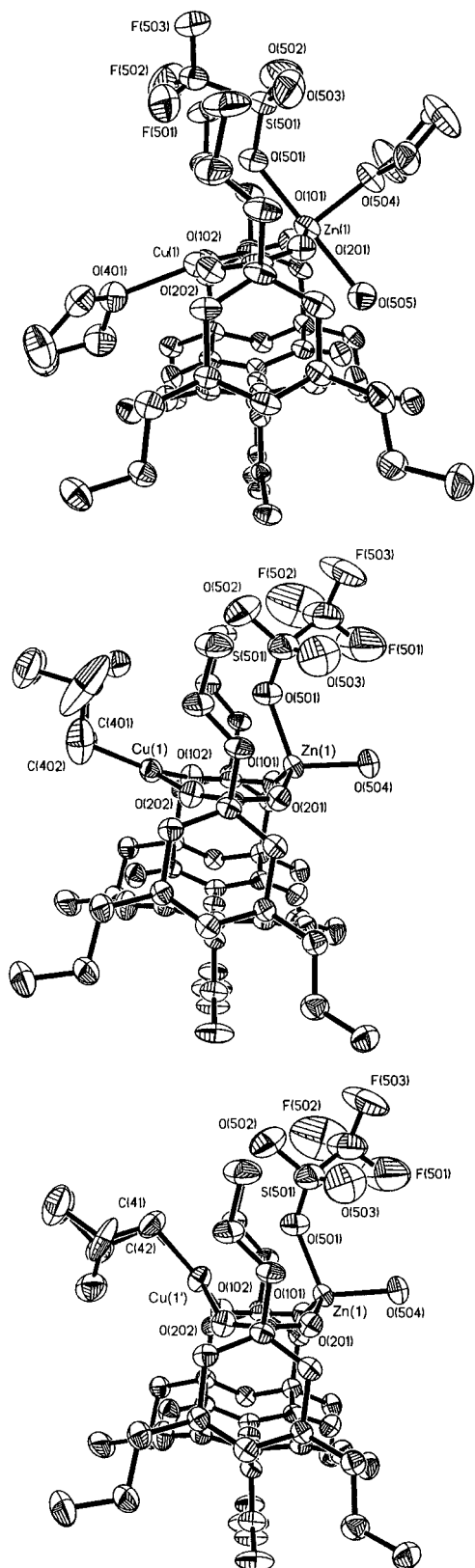


Figure 3. ORTEP diagrams with 50% thermal ellipsoids (top to bottom) of [CuZn(PXDK)(OTf)(THF)₂(H₂O)] (**9**), [CuZn(PXDK)(OTf)(NB)(H₂O)] (**11**, isomer A), and [CuZn(PXDK)(OTf)(NB)(H₂O)] (**11**, isomer B).

of the Cu(II) ion in **5** with Zn(II) or Fe(II) provided complexes with reasonably similar composition but of different structures, particularly with respect to the metal–metal separation. Collectively, these structural and copper(I) ligand exchange studies lend credence to the supposition that the short Cu–Cu distances

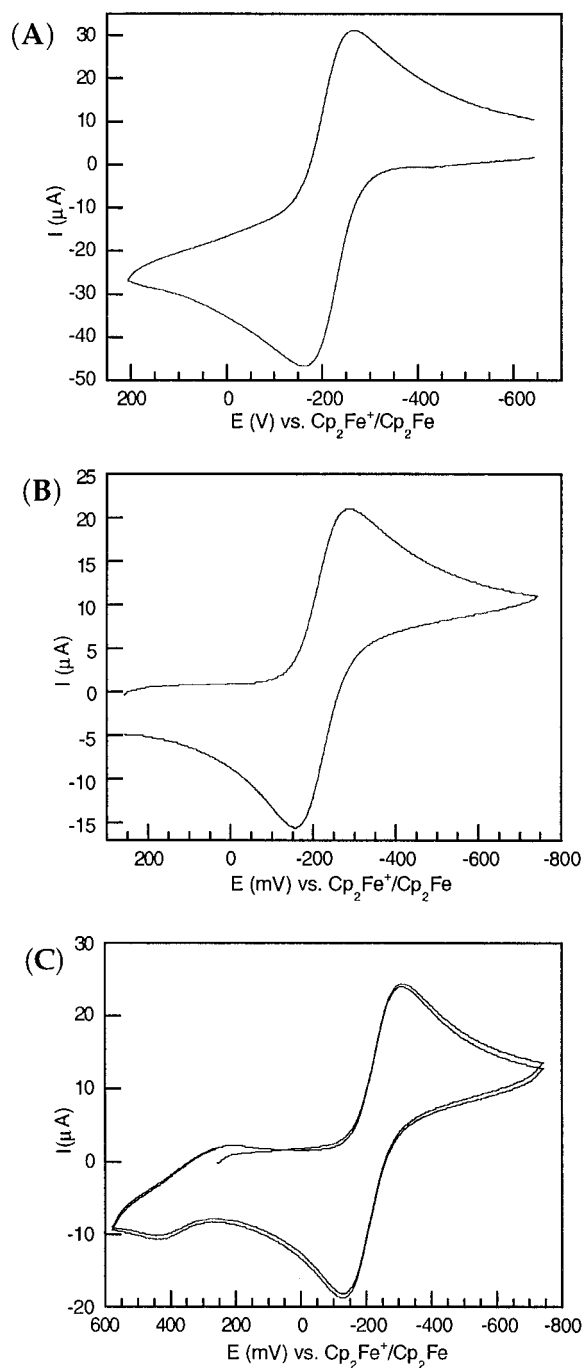
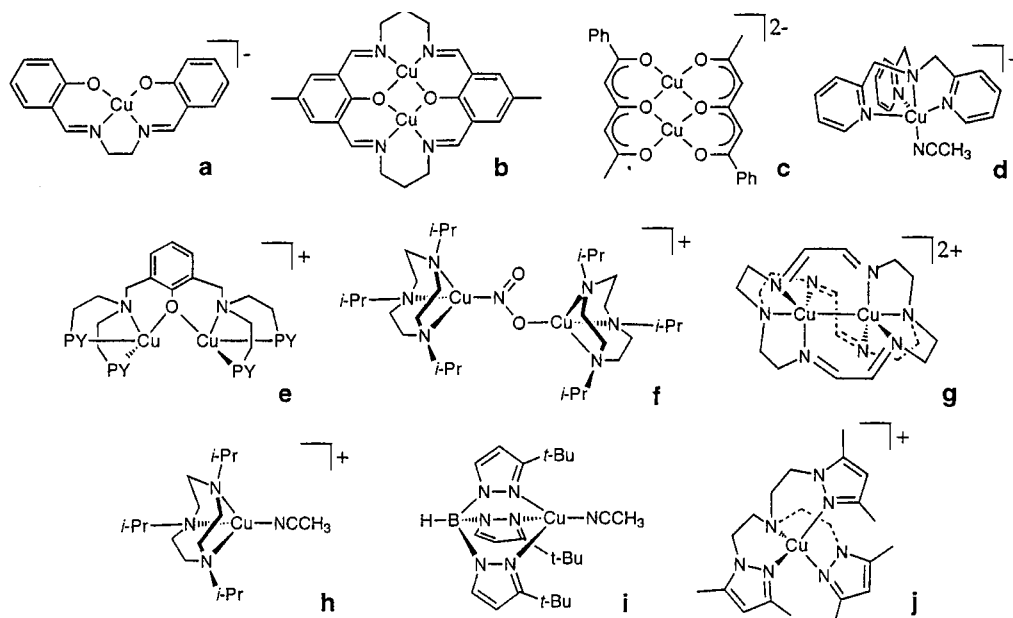


Figure 4. Cyclic voltammograms for (A) Cu₂(XDK), (B) [Cu₂(XDK)(THF)₄](BF₄) (**7**), and (C) [Cu₂(XDK)(*μ*-OTf)(THF)₂] (**4**, 2 cycles). All data were acquired with 10 mM complex, 0.5 M Bu₄NPF₆ as a supporting electrolyte, and a scan speed of 50 mV/s.

and approximate C_{2v} symmetry observed for **4–8** are a consequence of metal–metal bonding and valence delocalization, and not a function of the ligand architecture.

Electrochemical Properties of the Mixed-Valence Complexes. With the mixed-valence solvento complex **7** and the dicopper(I) analogue²⁹ in hand, we were interested to determine whether they could be electrochemically interconverted. It was anticipated a priori that quasireversible behavior might be observed owing to molecular reorganization, since the copper ion geometries in **7** and Cu₂(XDK) differ significantly. Moreover, it was of additional interest to determine whether the reduction potential of the [Cu₂(XDK)]⁺/Cu₂(XDK) couple deviates significantly from known trends for copper complexes

Table 4. Selected Electrochemical Data for a Range of Copper Redox Couples

entry	redox couple	electrolyte/solvent	lit ref elec	lit $E_{1/2}^a$	scaled $E_{1/2}^b$	ref
a	Cu ^{II} /Cu ^I	Pr ₄ NClO ₄ /0.1 M, DMF	SCE	–1210	–1770 ^c	54
b	(Cu ^{II} Cu ^I)/(Cu ^I Cu ^I)	Bu ₄ NClO ₄ /0.1 M, DMF	NHE	–517	–1318 ^d	18
c	(Cu ^{II} Cu ^I)/(Cu ^I Cu ^I)	Et ₄ NClO ₄ /0.1 M, DMF	SCE	–470	–1030 ^e	61
d	Cu ^{II} /Cu ^I	Bu ₄ NPF ₆ /0.2 M, DMF	Cp ₂ Fe ⁺ /Cp ₂ Fe, DMF	–628	–518 ^e	56
e	(Cu ^{II} Cu ^I)/(Cu ^I Cu ^I)	Bu ₄ NPF ₆ /0.2 M, DMF	Ag/AgNO ₃	–587	–497 ^f	59
f	(Cu ^{II} Cu ^I)/(Cu ^I Cu ^I)	Bu ₄ NPF ₆ /0.5 M, CH ₂ Cl ₂	SCE	+70	–490 ^e	60
7	(Cu ^{II} Cu ^I)/(Cu ^I Cu ^I)	Bu ₄ NPF ₆ /0.5 M, THF	Cp ₂ Fe ⁺ /Cp ₂ Fe, THF	–218	–218	this work
g	(Cu ^{II} Cu ^I)/(Cu ^I Cu ^I)	not given/DMF	Ag/AgCl	+310	–206 ^g	23
h	Cu ^{II} /Cu ^I	Bu ₄ NPF ₆ /0.5 M, MeCN	SCE	+360	–200 ^e	57
i	Cu ^{II} /Cu ^I	Bu ₄ NOTf/0.1 M, CH ₂ Cl ₂ /MeCN (9:1)	SCE	+910	+109 ^e	55
j	Cu ^{II} /Cu ^I	Bu ₄ NBF ₄ /0.1 M, MeCN	SCE	+690	+130 ^e	58

^a $E_{1/2}$ values are listed in mV. ^b All literature potentials have been scaled to Cp₂Fe⁺/Cp₂Fe in THF. ^c Cp₂Fe⁺/Cp₂Fe = +560 mV vs SCE in THF (see ref 63). ^d SCE = +241.2 mV vs NHE (see ref 62). ^e Cp₂Fe⁺/Cp₂Fe in DMF = –110 mV vs Cp₂Fe⁺/Cp₂Fe in THF (see ref 63). ^f Cp₂Fe⁺/Cp₂Fe = +20 mV vs Ag/AgNO₃ (see ref 56). ^g Ag/AgCl = –44.2 mV vs SCE (see ref 62).

because of the valence delocalized character of the mixed-valence form.⁵⁴

The homoleptic dicopper(I) complex exhibited a chemically reversible ($i_{pa}/i_{pc} \sim 1$) and electrochemically quasireversible ($\Delta E_p = 105$ mV, scan rate = 50 mV/s) cyclic voltammogram, with $E_{1/2} = -214$ mV vs Cp₂Fe⁺/Cp₂Fe (Figure 4A). Plots of i_{pa} and i_{pc} vs the square root of the scan rate are linear (Supporting Information), as would be expected for a (nearly) reversible couple. The same electrochemical couple was observed for the oxidized complex **7** (Figure 4B: $E_{1/2} = -222$ mV, $\Delta E_p = 132$ mV, scan rate = 50 mV/s, $i_{pa}/i_{pc} \sim 1$), confirming the one-electron nature of the process. An identical couple was also observed for the triflate complex **4** (Figure 4C: $E_{1/2} = -218$ mV, $\Delta E_p = 147$ mV, scan rate = 50 mV/s, $i_{pa}/i_{pc} \sim 1$), suggesting that triflate is dissociated upon dissolution in the electrolyte media, or upon reduction to the Cu^ICu^I species. At higher potentials an oxidation wave was detected, possibly signaling the existence of another species, with $E_{pa} = 443$ mV (Figure 4C). This feature could not be made reversible, even at high scan speeds (>500 mV/s). Unlike the behavior noted for the more weakly coordinating triflate anion, the trifluoroacetate ligand in **6** might remain associated with the {Cu₂(XDK)}⁺ fragment during cyclic voltammetry, because the analogous Cu^ICu^{II}/Cu^ICu^I reduction wave is completely irreversible.

To place the electrochemical data presented in a more general context, $E_{1/2}$ values for a variety of Cu^I and Cu^ICu^I complexes

are compiled in Table 4. In each case the redox couple was chemically reversible and electrochemically reversible, or nearly so ($\Delta E_p < 150$ mV). The mononuclear complexes listed contain ligands ranging from a dianionic N₂-bis(phenoxide) species in (**a**) to neutral^{55–58} donors with all nitrogen ligands (complexes **d**, **g–j**). For comparison to the results obtained for **7**, class I (**e**),^{59,60} II (**b**),¹⁸ and III (**g**)²⁴ mixed-valence systems with well behaved electrochemistry were included. For **c**, the mixed-valence form has not been isolated and characterized, but the dicopper(II) form undergoes two sequential one-electron steps at the same potential.⁶¹ To make the comparison more meaningful, potentials for each couple were referenced to the Cp₂Fe⁺/Cp₂Fe couple in THF. Scaling was accomplished with the aid of literature data relating SHE to SCE,⁶² AgCl/Ag to SCE,⁶²

(55) Tolman, W. B. *Inorg. Chem.* **1991**, *30*, 4877–4880.

(56) Wei, N.; Murthy, N. N.; Tyeklar, Z.; Karlin, K. D. *Inorg. Chem.* **1994**, *33*, 1177–1183.

(57) Mahapatra, S.; Halfen, J. A.; Wilkinson, E. C.; Pan, G.; Wang, X.; Young, V. G., Jr.; Cramer, C. J.; Que, L., Jr.; Tolman, W. B. *J. Am. Chem. Soc.* **1996**, *118*, 11555–11574.

(58) Sorrell, T. N.; Jameson, D. L. *Inorg. Chem.* **1982**, *21*, 1014–1019.

(59) Mahroof-Tahir, M.; Karlin, K. D. *J. Am. Chem. Soc.* **1992**, *114*, 7599–7601.

(60) Halfen, J. A.; Mahapatra, S.; Wilkinson, E. C.; Gengenbach, A. J.; Young, V. G., Jr.; Que, L., Jr.; Tolman, W. B. *J. Am. Chem. Soc.* **1996**, *118*, 763–776.

(61) Fenton, D. E.; Schroeder, R. R.; Lintvedt, R. L. *J. Am. Chem. Soc.* **1978**, *100*, 1931–1932.

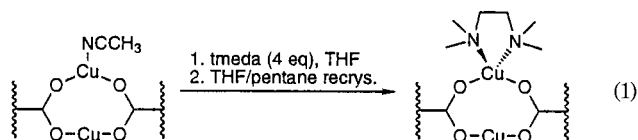
(62) Bard, A. J.; Faulkner, L. R. In *Electrochemical Methods Fundamentals and Applications*; John Wiley & Sons: New York, 1980.

(54) Patterson, G. S.; Holm, R. H. *Bioinorg. Chem.* **1975**, *4*, 257–275.

and SCE to $\text{Cp}_2\text{Fe}^+/\text{Cp}_2\text{Fe}$ (in THF).⁶³ These normalized $E_{1/2}$ values can be used as a rough approximation only, since the potentials for each complex depend on experimental conditions, including choice of solvent, electrolyte and electrolyte concentration, solvation, and ion pairing.

As expected from previous electrochemical studies of a large series of copper complexes,⁵⁴ the compounds in Table 4 display general trends. More negative reduction potentials occur as the ligand set becomes increasingly more basic, for ligands which favor square-planar or tetragonal over tetrahedral geometries, and with decreasing positive charge on the complex. From this standpoint all of the mixed-valence systems from the literature are unremarkable in the sense that their redox potentials are not anomalously affected by electronic coupling between adjacent copper atoms, except for **c**. Given the tetraanionic charge on the ligand and the rigidly planar structure of the dicopper(II) form, the $E_{1/2}$ values for this complex should more closely resemble that of **a**. Since little is known about the electronic and solid-state structures of the mixed-valence and dicopper(I) forms of **c**, however, it is difficult to rationalize these findings.

For the $\text{Cu}_2(\text{XDK})^+/\text{Cu}_2(\text{XDK})$ couple, two competing factors unique to this system can be identified which tend to shift the reduction potential in opposite directions. One is the stability of the mixed-valence form due to its delocalized electronic structure, and the other is the resistance of the dicopper(I) variant to deviate from its linear, two-coordinate copper geometries. Judging from the large positive deviation of the redox potential from its expected position in the series of complexes (Table 4), the latter feature seems to predominate. Our previous studies of ligand substitution reactions with the $\text{Cu}_2(\text{XDK})$ scaffold revealed one of the copper(I) ions to be unreactive toward σ -donors. Even when exposed to excess tetramethylethylenediamine (tmeda, eq 1), it preferred to retain a linear, two-



coordinate “skewed” geometry. We suggest that the electrochemical oxidation of $\text{Cu}_2(\text{XDK})$ reaction involves coordination of two THF ligands to each copper ion, thus making it more difficult to oxidize compared to the other copper complexes with anionic oxygen donors which do not have the geometrical constraints of XDK. In much the same way that ligands such as those in **i** and **j** prefer copper(I) by favoring a tetrahedral geometry, the XDK ligand enforces a linear, two-coordinate copper(I) structure. The magnitude of the positive $E_{1/2}$ shift appears to be much greater for **7**, however, since the all-oxygen $\text{Cu}_2(\text{XDK})$ donor set should place its $\text{Cu}^I\text{Cu}^{II}/\text{Cu}^I\text{Cu}^I$ potential near those found for **a–c**.

It is interesting that the $E_{1/2}$ value for $\text{Cu}_2(\text{XDK})$ falls in the range found for blue copper proteins, $\sim +200$ to $+800$ mV vs NHE (~ -600 to 0.0 mV vs $\text{Cp}_2\text{Fe}^+/\text{Cp}_2\text{Fe}$ in THF)^{64,65} and near the value of $+240$ mV vs NHE (~ -560 mV vs $\text{Cp}_2\text{Fe}^+/\text{Cp}_2\text{Fe}$ in THF) determined for the Cu_A domain of *Thermus thermophilus* cytochrome ba_3 .⁶⁶ Unlike our system, however,

these proteins employ a soft nitrogen/sulfur ligand donor set, and the rate of electron transfer is maximized at these biological centers by engineering minimal ligand reorganization when cycling between the +1 and +2 oxidation states. Here we have achieved biologically relevant redox potentials through geometric constraints, at the cost of imparting a significant degree of reorganizational energy.

EPR Studies of $[\text{Cu}_2(\text{XDK})(\text{THF})_4](\text{BF}_4)$ (7**).** EPR spectroscopy is a key tool for characterizing electronic exchange in mixed-valence copper complexes because seven-line hyperfine coupling of the unpaired electron to a pair of $I = 3/2$ copper nuclei is diagnostic of spin delocalization.^{16–18,21,24} In class II systems, electron exchange is typically mediated by population of vibrationally excited states, which imparts sufficient kinetic energy for the electron to pass over the barrier separating the electronic ground states of the two metal ions. Thus the rate of electron transfer in these systems is temperature-dependent, and valence delocalization is observed when the rate exceeds the time scale of the EPR experiment. In contrast, class III mixed-valence systems exhibit temperature-independent delocalization behavior, at least on the EPR time scale and over the temperature range to which the sample may be cooled. In this case the electronic structure is best defined by a single wave function encompassing both metal ions in which the unpaired electron resides. EPR studies of the present system were therefore undertaken in both the solid state and solution in order to probe the extent of electron delocalization, its temperature dependence, and the similarities between structures in the two different states.

A survey of the X-band frozen solution EPR spectra of **4**, **6**, and **7** obtained at liquid helium temperature proved them to be quite similar, so a detailed investigation was undertaken with the solvento adduct **7**. The X-band EPR spectra for **7** are presented in Figure 5 for frozen solution and powdered samples, respectively, together with a simulation for each case, from which g values and copper hyperfine coupling constants were derived. The spectra of **7** at 9 and 77 K exhibited nearly identical rhombic signals. A readily discernible seven-line copper hyperfine coupling pattern appeared on the lowest field component and overlapping hyperfine features on the two higher field components ($g_1 = 2.030$, $g_2 = 2.158$, $g_3 = 2.312$, $A_1^{\text{Cu}} = 20.0$ G, $A_2^{\text{Cu}} = 55.0$ G, $A_3^{\text{Cu}} = 122.5$ G). The X-band EPR spectra of powdered samples acquired at the same temperatures were extremely similar, albeit slightly broader, suggesting that the delocalized solid-state structure is retained in solution. A frozen solution Q-band spectrum acquired at 2 K also exhibited seven distinct hyperfine lines on the lowest field component (Figure 6). Furthermore, power dependence saturation studies on both the frozen solution and powdered samples revealed that each spectrum corresponded to a single species. Taken together, the EPR studies provide compelling evidence that the $\{\text{Cu}_2(\text{XDK})\}^+$ mixed-valence series should be classified as fully delocalized class III systems in both the solid state and solution. Moreover, these studies represent the first report of full delocalization for a dicopper mixed-valence species at 2 K, reinforcing its class III designation.

The rhombic signal and distinct hyperfine coupling constants at each g value were anticipated. The mixed-valence complexes have approximate C_{2v} symmetry, with significantly different ligand fields presented by the three types of ligands to each copper, the two carboxylate oxygens, the two THF oxygens, and the adjacent copper fragment.⁶⁷ The spectra may be

(63) Connelly, N. G.; Geiger, W. E. *Chem. Rev.* **1996**, *96*, 877–910.

(64) Reinhammar, B. R. M. *Biochim. Biophys. Acta* **1972**, *275*, 245–259.

(65) Tronson, D. A.; Ritchie, G. A. F.; Nicholas, D. J. D. *Biochim. Biophys. Acta* **1973**, *310*, 331–343.

(66) Immoos, C.; Hill, M. G.; Sanders, D.; Fee, J. A.; Slutter, C. E.; Richards, J. H.; Gray, H. B. *JBC*, **1996**, *1*, 529–531.

(67) Hathaway, B. J.; Billing, D. E. *Coord. Chem. Rev.* **1970**, *5*, 143–207.

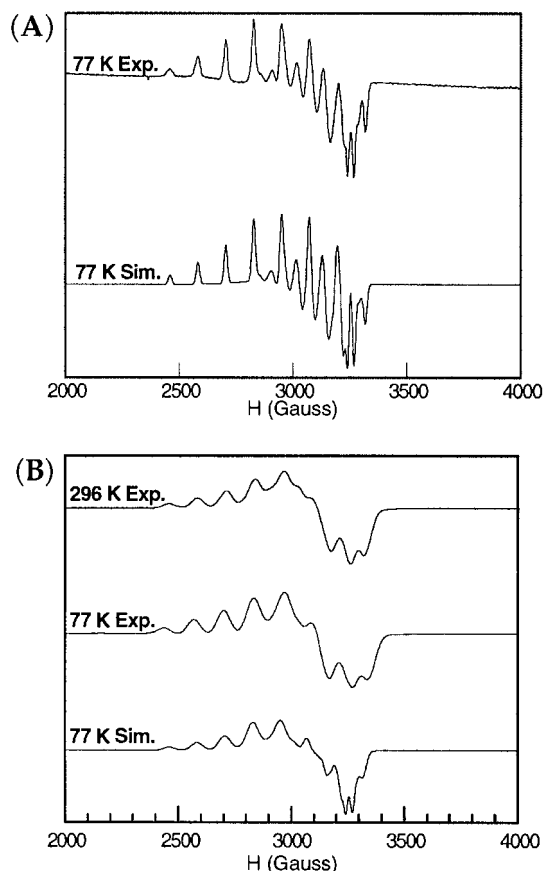


Figure 5. X-band EPR spectra for $[\text{Cu}_2(\text{XDK})(\text{THF})_4](\text{BF}_4)$ (**7**). (A) Frozen solution (1 mM in 2-Me-THF) at 77 K, experimental and simulated. (B) A powdered sample at 296 and 77 K, along with a simulation of the 77 K data.

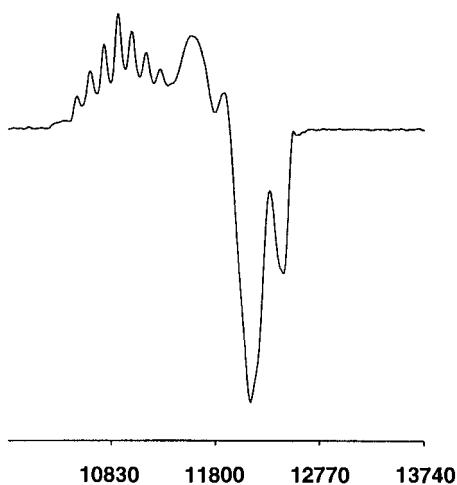


Figure 6. Q-band EPR spectrum for $[\text{Cu}_2(\text{XDK})(\text{THF})_4](\text{BF}_4)$ (**7**) in frozen solution (1 mM in 2-Me-THF) at 2 K.

compared with the rhombic spectra obtained for the Cu_A site⁶ and for $(\text{CuL}^i\text{PrdacoS})_2^+$,²¹ each of which showed similar g values to those obtained for **7**, but the bis(μ -thiolato) model complex exhibited substantially smaller copper hyperfine coupling constants (Table 1). The larger copper hyperfine interactions in **7** may be explained in part by a greater amount of spin density residing at the metal centers because of the short Cu–Cu interaction and the absence of a superexchange pathway through bridging ligands. In contrast to these rhombic systems, the octaazacryptand ligands afforded mixed-valence complexes with axial EPR spectra arising from its trigonal ligand field.

Molecular Orbital Calculations. An extended Hückel molecular orbital treatment of **7** was undertaken to elucidate its frontier molecular orbitals. The parameters of interest are the bonding and antibonding molecular orbitals responsible for the Cu–Cu interactions, their relative energies, and their copper orbital components. Net stabilization imparted to the dinuclear structure by Cu–Cu bonding was assessed by analyzing the interaction of the two mononuclear fragments as a function of Cu–Cu distance. Two simplified models were implemented, $[\text{Cu}_2(\mu\text{-O}_2\text{CCH}_3)_2(\text{OMe}_2)_4]$ and $[\text{Cu}_2(\text{OH})_2(\text{OH}_2)_2(\text{OMe}_2)_4]$, each derived from the crystallographic coordinates of the dicopper core in **8**. The z axis was taken along the apical copper– OMe_2 bond of one of the copper atoms, and the x and y axes along the copper–copper and copper–carboxylate (hydroxide/water) oxygen vectors, respectively.

The SOMO has considerable Cu $d_{x^2-y^2}$ /Cu d_{z^2} σ -antibonding character ($\sim 60\%$ for each copper), with a lobe from each metal pointed toward the other along the x axis.⁶⁸ The $4s$ ($\sim 11\%$ for each copper) and d_{z^2} ($\sim 8\%$ for each copper) orbitals also contribute significantly to the SOMO, having the same phases as the $d_{x^2-y^2}$ orbital on the two metals. In addition, the p orbital contribution from each ligand is out of phase with respect to the adjacent copper orbital lobe. The SHOMO in effect represents the bonding counterpart of the antibonding SOMO, but has more d_{z^2} (32%) and $4s$ (22%) character at the expense of the $d_{x^2-y^2}$ (36%). Again the ligand p orbitals are out of phase with respect to the adjacent copper orbital lobe, and in neither the SOMO nor the SHOMO are the carboxylate carbon atoms participating. An exchange pathway for electron delocalization therefore appears to be accessible only through the Cu–Cu interaction and not through the carboxylate ligands. Additional support for a net Cu–Cu bonding interaction is obtained from a reduced Mulliken overlap population analysis, which revealed the overall Cu–Cu overlap population to be $+0.1495$ at the crystallographic Cu–Cu distance of 2.40 Å. This value may be compared to the average overlap population of $+0.5362$ for C–O single bonds in the same structure. Hence the short Cu–Cu distance in the mixed-valence complexes is indicative of a weak metal–metal bond.

A fragment molecular orbital (FMO) analysis was carried out on $[\text{Cu}_2(\text{OH})_2(\text{OH}_2)_2(\text{OMe}_2)_4]$, a simpler model which permits the two copper fragments to be separated without breaking any carbon–oxygen bonds. The frontier molecular orbitals for this model had essentially identical energies and orbital contributions as those obtained for $[\text{Cu}_2(\mu\text{-O}_2\text{CCH}_3)_2(\text{OMe}_2)_4]$. The FMO analysis revealed that a significant bonding/antibonding interaction results between the highest occupied molecular orbital (HOMO) of the Cu(I) and Cu(II) fragments when the two are brought together. This interaction is also observed in a Walsh diagram, where the molecular orbital energy is plotted as a function of the Cu–Cu distance. The orbitals perturbed most dramatically are the SHOMO and SOMO, those suspected to play the greatest role in Cu–Cu bonding. The energy gap between the SOMO and SHOMO of $[\text{Cu}_2(\text{OH})_2(\text{OH}_2)_2(\text{OMe}_2)_4]$ is maximized at ~ 2.2 Å, reasonably close to the crystallographically determined distance of 2.40 Å. A minimum for the total energy of the molecular orbitals is reached at a Cu–Cu distance of ~ 2.9 Å. Greater error for this latter parameter is to be expected, since the total energy is made up of the individual energies of the 65 occupied molecular orbitals. Nevertheless, both the FMO and Walsh analyses support the idea that net

(68) See Supporting Information for contour plots of the SOMO and SHOMO and for the fragment molecular orbital and Walsh diagrams.

stabilization is imparted to these mixed-valence complexes through Cu–Cu bonding.

Conclusions

A series of dicopper mixed-valence complexes have been assembled with the XDK ligand system. Their fully delocalized, class III behavior has been demonstrated experimentally through (a) X-ray crystallographic studies which show that the coordination environments about each copper atom are identical and (b) solid state and solution EPR studies which demonstrate that the unpaired spin is coupled simultaneously to both $I = 3/2$ copper ions down to 2 K. Support for a stabilizing Cu–Cu bonding interaction in these complexes was provided by (a) the synthesis of Cu(I) heterodimetallic complexes with other divalent metal ions which are of similar composition but have much longer Cu^I···M^{II} distances; (b) the lack of reactivity of the mixed-valence complexes with norbornene, which reacts quantitatively with the Cu(I) fragment of the heterodimetallic complexes; and (c) extended Hückel molecular orbital calculations, which show a Cu–Cu interaction in the SOMO and SHOMO that is

composed primarily of Cu $d_{x^2-y^2}$ /Cu $d_{x^2-y^2}$ orbital overlap. Cyclic voltammetric studies revealed an electrochemically quasireversible Cu^ICu^{II}/Cu^ICu^I wave with a very positive $E_{1/2}$ value, tentatively attributed to the geometrical constraints imposed by the XDK ligand, which favors the linear two-coordinate Cu(I) geometry. In the aggregate, these studies significantly enhance our understanding of the assembly, stability, and electronic structure of class III mixed-valence Cu–Cu bonded systems.

Acknowledgment. This work was supported by grants from the National Science Foundation and AKZO Corp.

Supporting Information Available: Figures S1 and S2, fully labeled ORTEP diagrams for **9** and **11**; Figures S3 and S4, conductivity plots for **4** and **7**; Figures S5–S9, electrochemical plots; Figure S10, X-band EPR spectra for **7** at 9 K; Figures S11–S13, displaying plots derived from the extended Hückel molecular orbital calculations (38 pages). X-ray crystallographic files, in CIF format, for complexes **9** and **11** are available on the Internet only. Ordering and access information is given on any current masthead page.

IC980763B